Influence of deformation defects on the development of strain gradients during the tensile deformation of polyethylene

C. G'Sell* and N. A. Aly-Helal
Laboratoire de Physique du Solide (UA CNRS 155), Ecole des Mines, Parc de Saurupt, 54042 Nancy Cedex, France

and S. L. Semiatin
Battelle Memorial Institute, 505 King Avenue, Columbus, Ohio 43201-2693, USA

and J. J. Jonas
Department of Metallurgical Engineering, McGill University, 3450 University Street, Montreal, H3A 2A7, Canada
(Received 22 August 1990; accepted 13 December 1990)

The influence of initial deformation defects (localized prestrain) on the subsequent tensile behaviour of cylindrical bars of high-density polyethylene was investigated experimentally and theoretically. It was observed that neck nucleation occurs at the defect for moderate prestrains and outside the defect for larger prestrains. In the former case, the growth of the neck is limited and a secondary neck forms on the border of the predeformed zone. In all instances after the rod is fully drawn, a hard nodule remains at the defect location, the diameter of which increases with the prestrain. A simplified long-wavelength analysis proves that the above phenomena are controlled by the effect of the prestrain on the constitutive behaviour of the material. It is shown in particular that (i) prestraining softens the anelastic response of the polyethylene and (ii) prestraining hardens the material in the steady-state plastic regime. The complete stretching evolution of defect-containing samples can be modelled precisely by means of a finite-difference computer analysis.

(Keywords: polyethylene; stretching; plastic instability; necking; deformation defects)

INTRODUCTION

The control of unstable deformation is a difficult problem in industrial forming processes which involve the uniaxial or biaxial extension of ductile polymers[1–6]. Such operations include the cold drawing of fibres, thermoforming of plates and blow forming or stretching of thin films. Although the localized neck in these cases usually stabilizes at large strains owing to the gradual orientation of the macromolecules parallel to the tensile or stretch axes[7,8], the development of strain inhomogeneities may be responsible for unwanted fluctuations of the properties of the final product or, in extreme cases, for gross damage caused by localized adiabatic heating[9] or by the uncontrolled formation of crazes and flaws[10].

The possible sources of flow localization have been identified in the literature on plastic instability phenomena in metals[11–13] and in polymers[5,14,15]. It was shown in these studies that necking is likely to be initiated at (i) a geometric defect, which corresponds to a local reduction of the specimen cross section, (ii) a structural defect, at which the strength of the material is locally weaker, or (iii) a mechanical defect, where the material has undergone a local predeformation before beginning the extension. Although the first two types of flaws appear to be the most serious, the latter may also be responsible for inhomogeneous flow. One way in which a mechanical defect can arise in a workpiece is if it has been subjected to an accidental (or voluntary) predeformation by such means as a 'hammer blow' or plastic bending. However, the defect can also result from the residual strains developed during inhomogeneous cooling, such as occur in injection-moulded polymers. In all cases, the presence of a localized predeformation is likely to cause abrupt necking of the material during subsequent forming.

The aim of the present work was to clarify the effects of predeformation on the forming behaviour of a typical polymeric material, namely, high-density polyethylene (HDPE). To this end, experiments were conducted in which the kinetics of neck growth were recorded quantitatively. They consisted of tensile tests on specimens that had been subjected to previous local predeformations. The test results are summarized here in terms of the development of strain gradients as a function of the material properties and of the characteristics of the initial deformation. These data are employed to validate both a semiquantitative analytical interpretation of the necking phenomenon as well as a method for predicting neck shape based on a finite-difference computational approach.

* To whom correspondence should be addressed

0032-3861/92/061244-11

EXPERIMENTAL INVESTIGATION OF THE INFLUENCE OF PREDEFORMATION ON THE PLASTIC BEHAVIOUR OF HIGH-DENSITY POLYETHYLENE

Growth of necks in locally predeformed specimens subjected to uniaxial stretching

Cylindrical rods of polyethylene, 25 mm in diameter, were used in the experimental investigation. The high-density polyethylene (HDPE) is of the same grade (Union Carbide DFDY natural 77) as was used in previous work[14]. These rods were prepared by Plastifab Inc. of Montréal, Canada, by extrusion from the melt. This processing technique was preferred to injection moulding for it causes negligible molecular orientation.

Tensile specimens were prepared from this material in such a way that a small portion of the gauge length was characterized by a local predeformation but that it contained no geometric irregularity. Several operations were necessary to produce these specimens, as shown in *Figure 1*: (i) the extruded HDPE rod was machined on a lathe in order to reduce its diameter locally to $D_i = 16$ mm (*Figure 1b*); (ii) the rod was then pulled in tension at room temperature so that its diameter in the reduced region was equal to $D_p(X)$ (*Figure 1c*); (iii) a cylindrical tensile specimen of length $L_0 = 50$ mm was machined with a uniform diameter $D_0 = 8$ mm (*Figure 1d*). After this process, the specimen contained a localized prestrain $\varepsilon_p(X) = 2\ln(D_i/D_p(X))$, which could be determined quantitatively provided the profile $D_p(X)$ was recorded after the second operation. By this means, maximum prestrains of approximately 1.0 were readily obtained. It should be noted that this localized prestrain is similar in nature to the mechanical defects or 'hammer blows' discussed previously in the literature on plastic instability[11]. However, in the present case, there is no reduction of cross-sectional area associated with the local prestrain, because the profile was remachined after the predeformation.

The tensile specimens were subsequently pulled at room temperature (22°C) at a very slow engineering strain rate $\dot{\varepsilon}_e = \dot{L}/L_0 = 3.5 \times 10^{-4}\,s^{-1}$. *Figure 2* displays the engineering stress–strain curves obtained with mechanical defects of various amplitudes. The behaviour up to the maximum load is similar for all specimens except the most heavily predeformed one, which shows more gradual yielding. The minimum or steady-state load is reached earlier in specimens with larger prestrains. In addition, the plateau load is slightly higher in specimens with defects than in the sample without any defect.

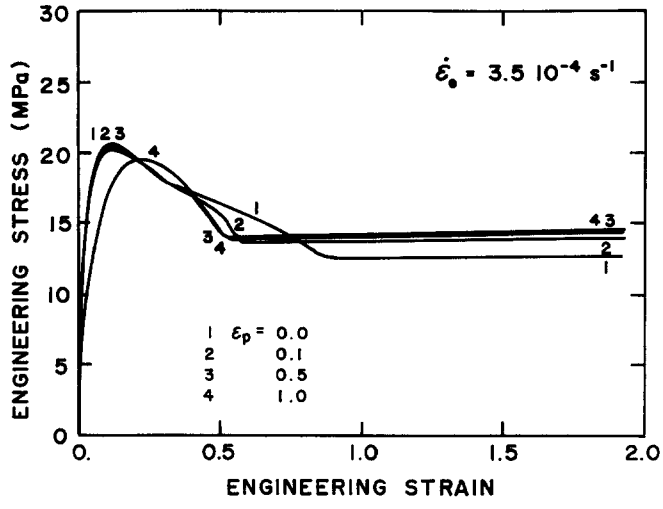

Figure 2 Influence of prestrain on the engineering stress–strain curves of high-density polyethylene. The specimens contained centrally predeformed zones with maximum predeformations of (1) 0.0, (2) 0.1, (3) 0.5 and (4) 1.0

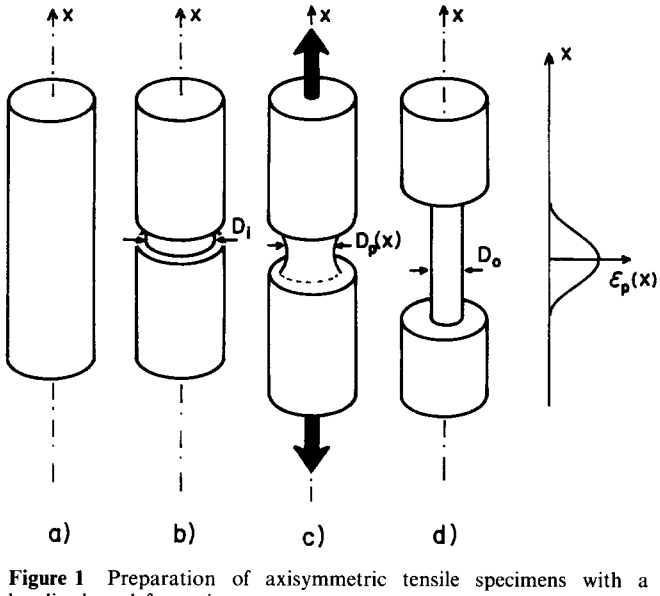

Figure 1 Preparation of axisymmetric tensile specimens with a localized predeformation

The most unexpected feature of the effect of mechanical defects was the shape of the necks that were produced (*Figure 3*). For the sample that had no initial defect (*Figure 3a*), the stretching remained apparently homogeneous to an engineering strain ε_e, of about 0.6, that is for a deformation much greater than the load maximum at $\varepsilon_e = 0.13$. A very diffuse neck then developed in the upper half of the specimen, in a zone that presumably contained a cross-section defect. Finally the shoulders of the neck propagated in the way noted in previous publications[14,15].

In the specimen with a maximum prestrain of 0.1 (*Figure 3b*), the neck appeared earlier (at $\varepsilon_e \simeq 0.1$) in the defect zone, although the cross-sectional area was *not* smaller in this region. However, the maximum strain did not continue to be located at the defect for very long. Instead, a *secondary neck* was initiated at the upper border of the prestrained zone and finally superseded the original neck at $\varepsilon_e \simeq 0.35$. This evolution is not readily visible to the naked eye, but microscopic analysis of the photographic films revealed it unambiguously. After the stabilization of this secondary neck, the shoulders propagated but not symmetrically: the upper shoulder moved first along the entire upper half of the sample before the lower one began propagating. After the neck propagation stage was completed, a slightly oversized bulge was observed to remain at the location of the original defect.

Similar phenomena are observed in *Figure 3c*, for a mechanical defect of 0.5, but with a much more dramatic amplitude. Necking was evident as early as $\varepsilon_e = 0.05$ at the location of the initial defect (in *Figure 3c*, it is clearly visible at $\varepsilon_e = 0.1$). Later, a secondary neck appeared at the edge of the defect (see *Figure 3c* at $\varepsilon_e = 0.4$), and its growth was very rapid. As in the preceding case, the neck began to propagate upwards, and finally downwards

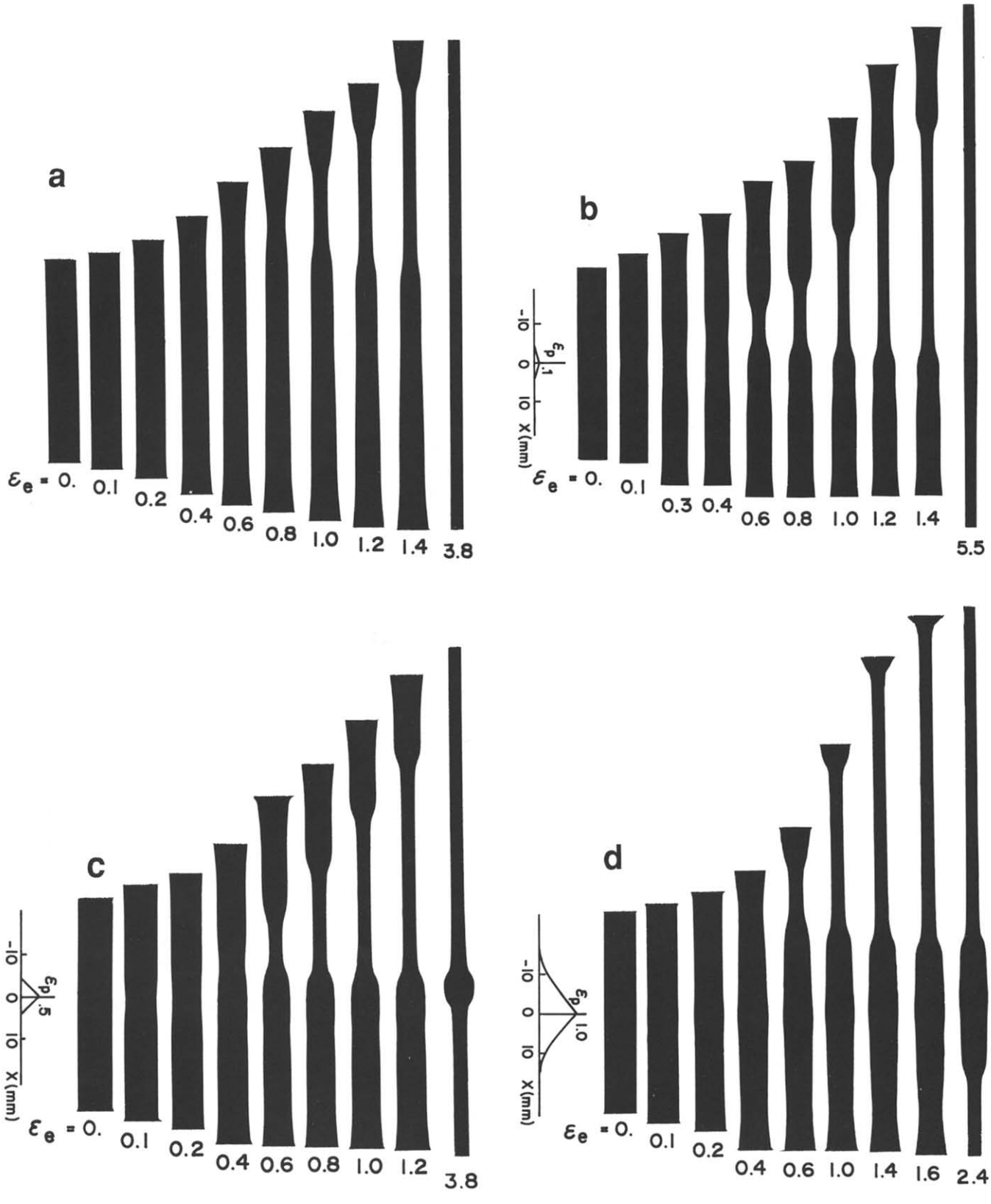

Figure 3 Kinetics of necking and cold drawing in specimens with central predeformations: (a) $\varepsilon_p = 0.0$, (b) $\varepsilon_p = 0.1$, (c) $\varepsilon_p = 0.5$, (d) $\varepsilon_p = 1.0$

from the defect. The bulge that remained in the centre of the stretched specimen had a very pronounced nodular shape.

In the last example, a sample with a maximum prestrain of 1.0 (*Figure 3d*), no necking whatsoever occurred at the initial defect. The plastic instability was initiated at the upper edge of the defect and then propagated into the regions that had not been predeformed. Subsequently, the second half of the sample experienced the necking process. In comparison to the case with $\varepsilon_p = 0.5$, a much larger final bulge was observed at the location of the predeformed region in this experiment.

The phenomenon illustrated by the above tests

demonstrates that an initial mechanical defect has two competing effects: (i) at small levels of prestrain, plastic flow is favoured at the defect, leading to preferential neck formation here; and (ii) at larger prestrains, the defect region is hardened to such an extent that the strain is concentrated in neighbouring portions of the specimen. These trends are quantified by the curves in *Figure 4*, which show the difference between the true strain at the defect ($\varepsilon_d = 2\ln(D_0/D_d)$) and the maximum true strain ($\varepsilon_s = 2\ln(D_0/D_s)$) in the secondary neck as a function of the nominal extension ε_e. In the strain calculations, D_d and D_s are the current diameter of the sample at the defect and at the smallest cross section of the secondary neck, respectively. The successive softening and hardening effects of a moderate prestrain are clearly observed from the curves for $\varepsilon_p = 0.1$ and 0.5, which show that the defect is subjected to the highest strain up to elongations of $\varepsilon_e \simeq 0.35$ and 0.3, respectively, after which the flow localizes in neighbouring portions that had no initial prestrain.

Determination of the intrinsic plastic behaviour of high-density polyethylene predeformed in tension

It has been demonstrated in previous papers[5,14,15] that the quantitative interpretation of necking and cold-drawing phenomena, such as those presented above, relies quite heavily on the accurate determination of the intrinsic plastic behaviour of the material. In the present case, therefore, it is important to know the influence of predeformation on the constitutive equation $\sigma(\varepsilon, \dot{\varepsilon})$, where σ, ε and $\dot{\varepsilon}$ are the true stress, true strain and true strain rate in uniaxial tension, respectively. For this purpose, a special tensile testing method was used in which a constant true strain rate is imposed in the centre of an hourglass-shaped specimen. This technique, described at length elsewhere[16], makes use of a diametral strain transducer, a hydraulic closed-loop tensile testing machine and a special servo-controller equipped with an exponential function generator.

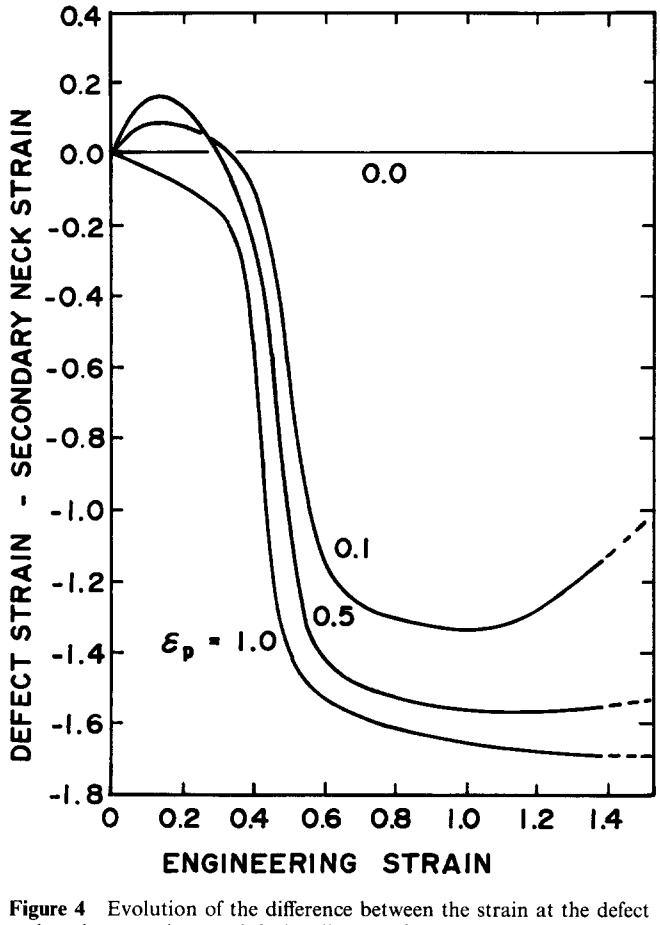

Figure 4 Evolution of the difference between the strain at the defect and at the secondary neck in locally predeformed samples

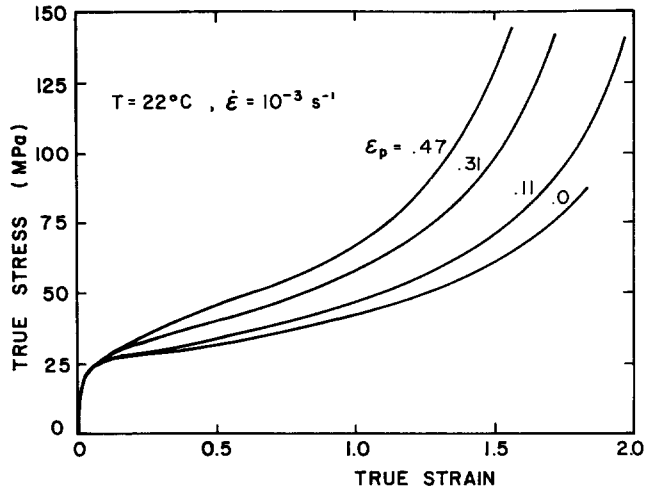

Figure 5 Influence of tensile predeformation on the true stress–strain behaviour of high-density polyethylene at 22°C

Hourglass-shaped specimens were machined from polyethylene rods that had been predeformed by extension in the same way as discussed above. Prestrains in the range $\varepsilon_p = 0$ to $\varepsilon_p = 0.47$ were imposed. These samples were then tested at room temperature (22°C) and a constant true strain rate $\dot{\varepsilon} = 10^{-3}\,s^{-1}$.

The true stress–true strain curves of predeformed samples are displayed in *Figure 5*. In these graphs, 'true strain' is the apparent strain $\varepsilon = 2\ln(D_0/D)$, where D_0 is the initial minimum diameter of the hourglass-shaped specimen and D its minimum diameter during the tensile test. It is evident that predeformation has a strong influence on the tensile behaviour of polyethylene in the range of large plastic strains. The flow stress increases gradually with increasing prestrain (about 40% increase of flow stress at $\varepsilon = 1.2$). Furthermore, it is of importance to note that the effect of predeformation is somewhat different for the initial portion of the stress–strain curves. Essentially, the anelastic* transition of predeformed polyethylene is *more progressive* than that of the virgin material. Flow curves for prestrained material were also obtained from tests conducted at several different strain rates. From these experiments, it was found that the strain-rate sensitivity coefficient of the high-density polyethylene, $m = (\partial \ln \sigma / \partial \ln \dot{\varepsilon})_\varepsilon$, is equal to about 0.075. As observed in a previous paper[14], the influence of strain (or prestrain) on this coefficient can be neglected to a first approximation.

THEORETICAL MODELLING OF THE DEVELOPMENT OF NECKS IN PREDEFORMED POLYETHYLENE RODS SUBJECTED TO STRETCHING

The experimental results described above will now be discussed theoretically. The approach will be twofold.

* Here the elastic-to-plastic transient stage is called 'anelastic'; it is sometimes referred to as 'viscoelastic' or 'pre-yield' behaviour in some publications

On the one hand, the effect of a localized predeformation on unstable flow in polyethylene will be interpreted on the basis of the standard 'long-wavelength' theory of plastic instability in uniaxial tension[11]. This approach is used to gauge the growth of a diffuse neck in a round tensile specimen in terms of the development of strain gradients. On the other hand, numerical simulations will also be presented. Such simulations yield quantitative predictions of the evolution of the neck profile and the load–extension curve for a tensile bar with a localized predeformation. In both the analytical and numerical approaches, the effect of predeformation will be introduced through its influence on the constitutive equation of the material. This influence will be discussed first.

Constitutive equation of predeformed high-density polyethylene

It has been shown in a previous paper[17] that the flow stress of polyethylene at room temperature is mainly determined by the total strain and by the current strain rate. If a tensile sample is unloaded for a given period of time and then reloaded, however, it is observed that the reloading flow curve rejoins the uninterrupted one after a short anelastic transient. Thus, according to several authors (e.g. ref. 18), it is possible to take the effect of a predeformation into account in an approximate manner by the simple addition of the prestrain ε_p to the current strain ε in the constitutive law, except for the initial anelastic regime.

The above conclusion is supported by the construction in *Figure 6*, corresponding to several predeformed polyethylene samples, where the stress–strain curves have been shifted along the strain axis by an amount equal to the value of the prestrain. Within the range of experimental error, all the curves for the prestrained materials coincide with the curve for the sample without any predeformation. It appears, therefore, that the total accumulated strain can be used as a state variable to describe the deformation kinetics. This is not surprising inasmuch as the amount of mean molecular orientation has been found to correlate well with the strain[7].

In a previous paper[16], it was shown that the constitutive relation for high-density polyethylene could be written in the form:

$$\sigma(\varepsilon, \dot{\varepsilon}) = K[1 - \exp(-w\varepsilon)] \exp(h\varepsilon^2)\dot{\varepsilon}^m \qquad (1)$$

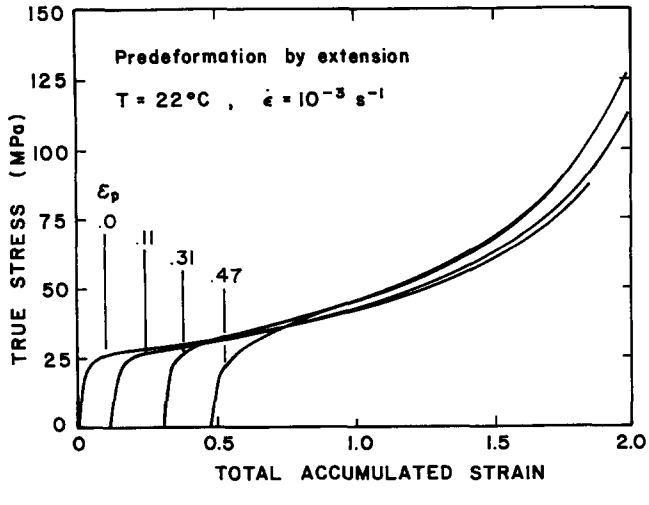

Figure 6 Master flow curve obtained by the horizontal translation of the true stress–strain curves of *Figure 5* by the corresponding prestrain

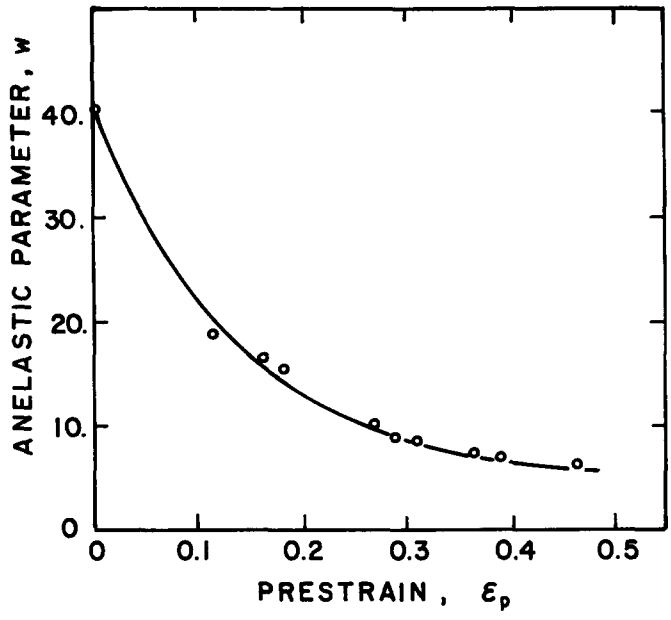

Figure 7 Influence of prestrain on the anelastic parameter w of the constitutive relation of high-density polyethylene

where the term in square brackets represents the transient anelastic behaviour, the $\exp(h\varepsilon^2)$ term describes the plastic strain hardening and $\dot{\varepsilon}^m$ takes into account the strain-rate sensitivity. The material constants were evaluated by fitting the experimental data, and found to take the values $K = 46$ MPa, $w = 40$, $h = 0.41$ and $m = 0.075$, respectively.

From the construction of *Figure 6*, it is clear that the constitutive equation of predeformed specimens then becomes:

$$\sigma(\varepsilon, \dot{\varepsilon}, \varepsilon_p) = K\{1 - \exp[-w(\varepsilon_p)\varepsilon]\} \exp[h(\varepsilon + \varepsilon_p)^2]\dot{\varepsilon}^m \qquad (2)$$

in which the strain shift due to ε_p is apparent in the hardening term $\exp[h(\varepsilon + \varepsilon_p)^2]$. The curves in *Figure 6* reveal that the anelastic transition of predeformed materials is more gradual than in the original polyethylene. This effect is quantified by the decrease in the anelastic parameter $w(\varepsilon_p)$, whose dependence on the prestrain is illustrated in *Figure 7**. This enhancement of the anelastic compliance by predeformation can be ascribed to a specific macromolecular mechanism. It has been shown, for example in refs. 19 and 20, that, once the crystallites in polyalkenes such as polyethylene and polybut-1-ene are sheared, rotated and eventually fragmented under the effect of a predeformation, the material assumes a somewhat more amorphous rubberlike state. This occurs because the glass transition temperature of the polymers indicated above is below room temperature. The softer anelastic behaviour of the predeformed polymer is then due to these flexible molecules extracted from the original crystallites.

Uniaxial analysis of flow localization in predeformed tensile specimens

The growth of necks in metallic tensile specimens with deformation defects has been discussed previously[12,21,22].

*The value of $w(\varepsilon_p)$ was determined from the curves of *Figure 6* by a procedure similar to the one utilized in ref. 16. First the master curve at a reference strain rate was obtained by best fitting the m coefficient. Then, the h parameter was deduced from the slope of the $\ln(\sigma/\dot{\varepsilon}^m)$ vs. $(\varepsilon + \varepsilon_p)^2$ plot. Finally, the anelastic stage was fitted with the $1 - \exp[-w(\varepsilon_p)\varepsilon]$ function to provide the appropriate value of $w(\varepsilon_p)$

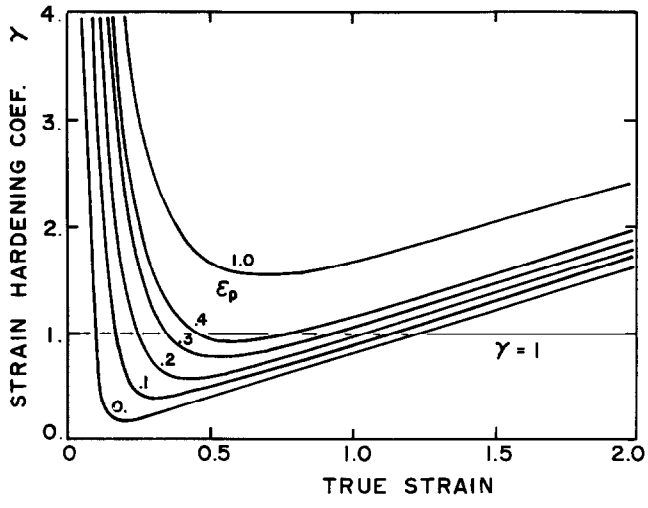

Figure 8 Influence of predeformation on the strain hardening coefficient γ of high-density polyethylene, as given by equation (7)

In these studies, the predeformation under consideration corresponded to a form of mechanical damage such as that induced by a 'hammer blow'[11]. This kind of defect was therefore associated with (i) a local prestrain $\varepsilon_p(X)$ and (ii) a corresponding reduction of cross-sectional area $A(X)=A_0\exp[-\varepsilon_p(X)]$, where A_0 is the area of the sample before the introduction of the deformation defect. The modelling of flow localization in such specimens was treated on the basis of the 'long-wavelength' approximation; that is to say, the assumption of a uniaxial stress state and the neglect of the effects of triaxiality during necking. It was concluded that locally predeformed zones in metals act as preferential sites for necks, and thus should be avoided in order to promote the homogeneous stretching of bars and sheets.

The experimental results presented in this paper are related to a somewhat different situation: (i) the predeformation and the cross-section reduction are introduced *independently* of each other, and (ii) the flow stress for the polymeric material under investigation is characterized by an *exponential increase* at large strains, a behaviour greatly different from the saturation flow stress observed for most metals.

With this as background, consider an axisymmetric tensile specimen of polyethylene that has been subjected to an arbitrary distribution of prestrain $\varepsilon_p(X)$ along its axis (here, X represents the *Lagrangian*, or material, coordinate). The specimen is remachined after the predeformation is applied in such a way that the axial variation in the cross section is $A_0(X)$. In the following derivation, the 'true' strain at a given material cross section X is defined as:

$$\varepsilon(X)=\ln[A_0(X)/A(X)] \tag{3}$$

With this definition, $\varepsilon(X)$ represents the apparent strain experienced by the specimen after it has been remachined†.

† The definition introduced here contrasts with that of previous papers which have dealt with the total strain $\varepsilon_T(X)=\varepsilon_p(X)+\varepsilon(X)$ accumulated during the entire history of the material. It is preferable for predicting the consequences of a hypothetical mechanical defect in a workpiece subjected to plastic deformation. It is of interest to note that, in most practical cases, the predeformation is imposed on the material during its processing and that it is actually machined afterwards. Therefore, the prestrain distribution is not usually known and $\varepsilon(X)$ is the only strain that can be measured in practice

We are now in a position to discuss the long-wavelength analysis. According to the usual procedure[13], the equilibrium equation (where P is the axial load) at a fixed time t can be written as:

$$\frac{\mathrm{d}\ln P}{\mathrm{d}X}=\frac{\mathrm{d}\ln\sigma}{\mathrm{d}X}+\frac{\mathrm{d}\ln A}{\mathrm{d}X}=0 \tag{4}$$

The axial tensile stress σ is a function not only of the axial strain ε and strain rate $\dot{\varepsilon}$ but also of the local prestrain ε_p:

$$\left(\frac{\partial\ln\sigma}{\partial\varepsilon}\right)_{\varepsilon_p,\dot{\varepsilon}}\frac{\mathrm{d}\varepsilon}{\mathrm{d}X}+\left(\frac{\partial\ln\sigma}{\partial\ln\dot{\varepsilon}}\right)_{\varepsilon,\varepsilon_p}\frac{\mathrm{d}\ln\dot{\varepsilon}}{\mathrm{d}X}+\left(\frac{\partial\ln\sigma}{\partial\varepsilon_p}\right)_{\varepsilon,\dot{\varepsilon}}\frac{\mathrm{d}\varepsilon_p}{\mathrm{d}X}+\frac{\mathrm{d}\ln A}{\mathrm{d}X}=0 \tag{5}$$

In this equation several derivatives are of particular significance: $\mathrm{d}\varepsilon/\mathrm{d}X=\lambda$ is the strain gradient in Lagrangian coordinates, $\mathrm{d}\ln\dot{\varepsilon}/\mathrm{d}X=\mathrm{d}\lambda/\mathrm{d}\varepsilon=\lambda'$ is the strain-rate gradient, $\mathrm{d}\varepsilon_p/\mathrm{d}X=\lambda_p$ is the prestrain gradient, $\mathrm{d}\ln A/\mathrm{d}X=\mathrm{d}\ln A_0/\mathrm{d}X-\lambda$ is the cross-sectional area gradient, $(\partial\ln\sigma/\partial\varepsilon)_{\varepsilon_p,\dot{\varepsilon}}=\gamma(\varepsilon,\varepsilon_p)$ is the strain hardening coefficient, $(\partial\ln\sigma/\partial\ln\dot{\varepsilon})_{\varepsilon,\varepsilon_p}=m$ is the strain-rate sensitivity coefficient, and $(\partial\ln\sigma/\partial\varepsilon_p)_{\varepsilon,\dot{\varepsilon}}=\gamma_p(\varepsilon_p,\varepsilon)$ is the prestrain hardening coefficient.

With the above definitions, equation (5) can be rewritten in the form:

$$m\lambda'=(1-\gamma)\lambda-\mathrm{d}\ln A_0/\mathrm{d}X-\gamma_p\lambda_p \tag{6}$$

In the present work, λ is taken to be positive when X is directed towards the centre of the neck; therefore, $(-\mathrm{d}\ln A_0/\mathrm{d}X)$ is also positive at a geometric defect.

From the constitutive equation for HDPE, the strain hardening coefficient is found to be:

$$\gamma(\varepsilon_p,\varepsilon)=\frac{w(\varepsilon_p)}{\exp[w(\varepsilon_p)\varepsilon]-1}+2h(\varepsilon+\varepsilon_p) \tag{7}$$

and the prestrain hardening coefficient is given by:

$$\gamma_p(\varepsilon_p,\varepsilon)=\frac{\varepsilon}{\exp[w(\varepsilon_p)\varepsilon]-1}\frac{\partial w}{\partial\varepsilon_p}+2h(\varepsilon+\varepsilon_p) \tag{8}$$

The evolution of γ with true strain is illustrated in *Figure 8* for different amounts of prestrain. It is evident that the strain hardening coefficient increases with increasing ε_p. Furthermore, this evolution is different at different values of ε since, at small strains, the increase in γ is mainly controlled by the anelastic term of equation (7), while at large strains it is the 'stready-state' term that controls the (small) increase in γ. Since the anelastic response has a significant effect only at small strains, the curves in *Figure 8* differ mostly in their initial portions for equivalent ε values. It is also of interest to note that, for large prestrains, γ barely drops below the value $\gamma=1$. The two strains at which $\gamma(\varepsilon)$ assumes this particular level correspond, after Considère[23], to the occurrence of tensile load extrema and have been shown to characterize the onset and completion of rapid flow localization at constant strain rate[11].

The evolution of γ_p with prestrain (equation (8)) is depicted in *Figure 9* for different amounts of strain. It is evident that the effect of predeformation on γ_p depends not only on ε_p but also on ε. In the expression for γ_p, equation (8), the first term is negative owing to $\mathrm{d}w/\mathrm{d}\varepsilon_p$ while the second term is positive. Thus the γ_p coefficient

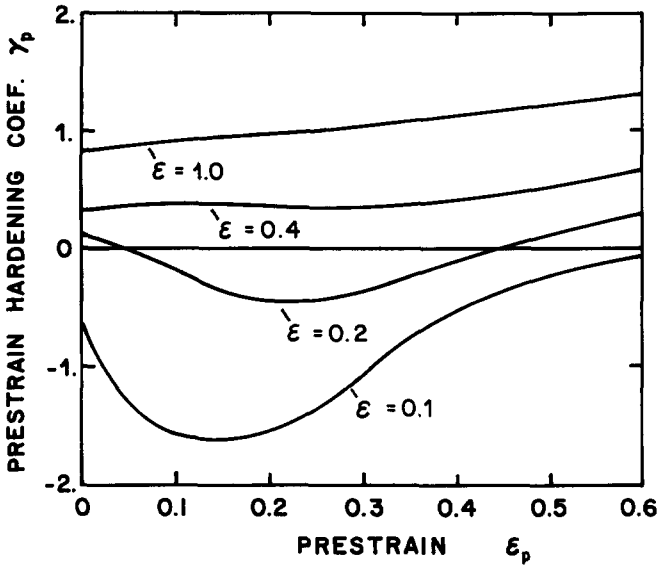

Figure 9 Influence of prestrain on the prestrain hardening coefficient γ_p, of high-density polyethylene, as given by equation (8)

represents a *softening* effect at small strains and a *hardening* effect at large strains.

By integration of equation (6), the evolution of the apparent strain gradient at the defect was computed for the experiments considered in the second section. The evolution of λ is of interest since it describes the kinetics of flow localization at a given material location in the sample. Increasing positive values of λ correspond to the growth of a neck, while a decrease in λ represents the healing of strain inhomogeneities. In the results described below, the Lagrangian gradient λ was transformed into its corresponding value λ_E calculated in Eulerian or laboratory coordinates by the simple relation $\lambda_E = \lambda \exp(-\varepsilon)$. This was done because λ_E better represents the observed evolution of the specimen, since it takes into account the local elongation of the material while the Lagrangian strain gradient λ does not[15].

In the case of an ideal mechanical defect corresponding to a local predeformation without a geometric inhomogeneity (*Figure 1*), differential equation (6) reduces to the following expression:

$$m\lambda' = (1-\gamma)\lambda - \gamma_p \lambda_p \qquad (9)$$

where λ_p was determined experimentally from the profile $D_p(X)$ of the predeformed sample before remachining (*Figure 1c*) using the relation:

$$\lambda_p = -d\varepsilon_p/dX = [2/D_p(X)][dD_p(X)/dX]$$

It was found in the experiments that $\varepsilon_p(X)$ was roughly linear, yielding typical values of λ_p of about $0.05\,mm^{-1}$. With this value of λ_p, equation (9) was integrated numerically for different prestrains ranging from 0.1 to 1.0 and with the material coefficients γ and γ_p given by equation (7) and (8), respectively.

The resulting evolution of the Eulerian strain gradient λ_E with true strain for several values of ε_p is illustrated in *Figure 10*. It is clear that the amount of local prestrain is an important parameter. After a small prestrain ($\varepsilon_p = 0.1$), a positive strain gradient grows *ab initio*, although it accelerates rapidly only after $\varepsilon \simeq 0.3$. This strain corresponds approximately to the moment when γ first passes through the critical value $\gamma = 1$ (*Figure 8*). It is only at $\varepsilon \simeq 1$, when γ passes through the critical value for the second time (*Figure 8*), that the flow localization saturates and finally decreases to zero as the macromolecules rearrange into a hard fibre-like texture. By contrast, the curves for $\varepsilon_p = 0.2$ or $\varepsilon_p = 0.3$ show that the strain range for which the inhomogeneity grows is very narrow. Above $\varepsilon = 0.5$, the gradient λ_E decreases and takes on negative values. This corresponds to the situation where a secondary neck is developed away from the region containing the initial deformation defect. The extreme case is illustrated by the curve for $\varepsilon_p = 1$. In this instance, the mechanical defect no longer acts as a neck initiator but rather as a strain-resistant portion at which a hard nodule is formed from the beginning of the experiment, thereby leading to a negative strain gradient. On a qualitative basis, it is therefore evident that the curves of *Figure 10* explain very well the experimental observations displayed in *Figure 3* and the data of *Figure 4*.

Introduction of the effects of stress triaxiality in the theoretical model

The analytical derivation presented above is of considerable interest since it points out the significant material parameters that control flow localization in predeformed specimens. Nevertheless, the specific quantitative results are only of limited applicability for the following three reasons:

(i) The strain gradient curves displayed in *Figure 10* represent the evolution of λ_E at a given material element in a tensile specimen and thus illustrate solely how the *local* slope of the sample profile evolves during stretching. Instead, it is of interest to model the changes in the entire profile, including the growth of the neck and the propagation of its shoulders, in order to simulate the experiments more closely.

(ii) The strain-rate distribution cannot be readily derived from the analytical treatment. Consequently, the autographic load–extension curves cannot be obtained in straightforward computations.

(iii) In all the tension experiments performed at room temperature under isothermal conditions, the maximum strain gradient is always less than about $0.5\,mm^{-1}$ (see for example *Figure 3*). By contrast, it is evident from

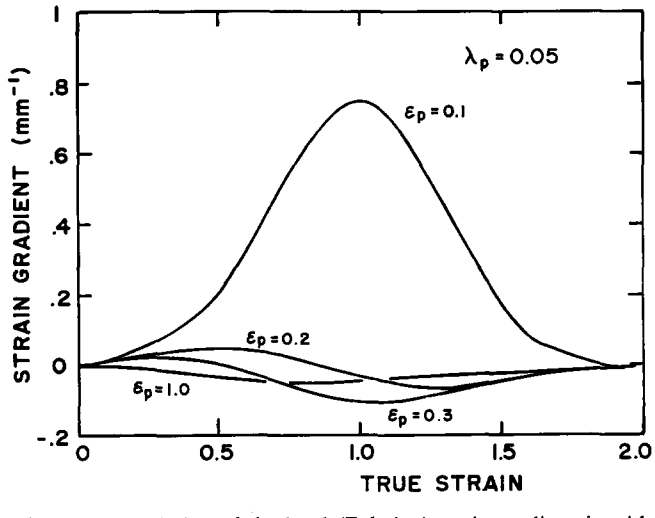

Figure 10 Evolution of the local (Eulerian) strain gradient λ_E with true strain ε in a high-density polyethylene sample subjected to increasing localized predeformations. The evolution caused by four local prestrains is shown for the region of predeformation

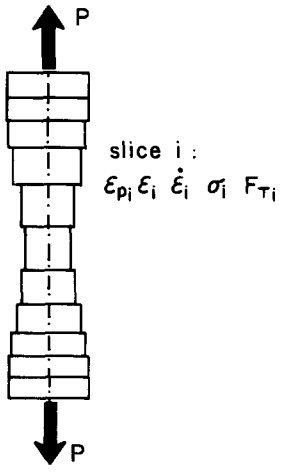

Figure 11 Finite-difference discretization of the tensile specimen

Figure 10 that the uniaxial analysis predicts values of λ_E that are much too large.

The deficiency cited in (iii) has been discussed at length previously[24]. There, it was demonstrated that the source of the discrepancy can be attributed to the effect of stress triaxiality on the flow stability. It was shown that non-axial components of stress appear in the portions of the specimen that exhibit significant non-zero profile curvatures. Consequently, the mean effective stress σ_{eff} in the specimen cross sections at which the profile curvature is convex is greater than the mean axial stress σ, while it is less where the curvature is concave (e.g. at the centre of the neck). Thus, the triaxiality effect tends to reduce the sharpness of the strain inhomogeneities.

The effect of stress triaxiality can be incorporated formally into the equilibrium differential equation (equation (4)) by introducing the supplementary term $(-\mathrm{d}\ln F_T/\mathrm{d}X)$ on the right-hand side, where $F_T=\sigma_{eff}/\sigma$ is called the 'triaxiality factor'. In the round bar case, it has been demonstrated[25] that a practically useful expression for F_T is given, to a first approximation, by the Bridgman formula[26]:

$$F_T=1/\{[1+(2R_c/R)]\ln[1+(R/2R_c)]\} \qquad (10)$$

where R and R_c are the local radius and the local radius of curvature of the specimen profile, respectively. If the triaxiality term is introduced into equation (9), however, the simple integration to obtain $\lambda(\varepsilon)$ is no longer possible since the radius of curvature R_c itself depends non-linearly on the local values of ε, λ and λ'. Hence, numerical methods must be employed to establish the kinetics of flow localization.

Description of the computer program

The evolution of the specimen profile, as well as the engineering stress–strain curve, were predicted by means of a finite-difference simulation that incorporates all the ingredients introduced in the preceding sections.

(i) A one-dimensional geometry is used, in which the specimen is decomposed into N slices, each normal to the axis. Each individual element is assumed to deform homogeneously (*Figure 11*).

(ii) The material behaviour is modelled using the isothermal constitutive equation, which relates the mean effective stress to the strain, strain rate and prestrain in each slice.

(iii) The external boundary conditions are specified by assuming (a) a constant overall elongation rate and (b) a zero strain rate for the material elements located at the ends of the sample gauge section.

(iv) The force equilibrium condition is expressed by the constancy of the load along the sample, and incorporates the flow stress, cross-sectional area and triaxiality factor F_T in each slice. Incorporation of the F_T factor maintains the simplicity of a one-dimensional analysis but produces simulation predictions that are more accurate than those based on the conventional long-wavelength assumption. The equilibrium equation is used to determine the strain-rate distribution throughout the sample.

(v) A finite-difference scheme is used in which the strain increments, for each slice, are computed from the current distribution of the strain rates in all the elements.

The computer code written to carry out the numerical calculations is similar to those described in other papers[27–29] for the study of necking in metals or polymer tensile specimens. Thus, only a brief description of particular features of the program is given below.

The total elongation rate $\dot{L}$ of the discretized sample depends on the elongation rate $\dot{L}_i$ of all the elements:

$$\frac{\dot{L}}{L_0}=\sum_{i=1}^{N}\frac{\dot{L}_i}{L_0}=\sum_{i=1}^{N}\frac{L_{0i}}{L_0}\exp(\varepsilon_i)\dot{\varepsilon}_i \qquad (11)$$

This elongation rate is held constant during the entire tension simulation. Furthermore, because the strain rates considered in the present work are very low, inertia effects are negligible, and the applied load P is assumed to be transmitted along the specimen. The discretized form of the equilibrium equation for each element is thus:

$$P=\sigma_i A_i=\sigma_{eff\,i}A_i/E_{Ti}=\text{const} \qquad (12)$$

The constitutive equation is:

$$\sigma_{eff}=K[1-\exp(-w_i\varepsilon_i)]\exp(h\varepsilon_i^2)\dot{\varepsilon}_i^m \qquad (13)$$

In this last relation, the anelastic parameter w_i varies from element to element according to the local value of the prestrain ε_{pi} applied to the given slice prior to testing. The $w_i(\varepsilon_{pi})$ dependence is displayed in *Figure 7*.

Equations (11), (12) and (13) can be combined to give the strain rate in the ith element explicitly:

$$\dot{\varepsilon}_i=\frac{\dot{L}}{L_0}\left[\sum_{j=1}^{N}\frac{L_{0j}}{L_0}\exp(\varepsilon_j)\left(\frac{A_i}{A_j}\frac{1-\exp(-w_i\varepsilon_i)}{1-\exp(-w_j\varepsilon_j)}\times\frac{\exp(h\varepsilon_i^2)}{\exp(h\varepsilon_j^2)}\frac{F_{Tj}}{F_{Ti}}\right)^{1/m}\right]^{-1} \qquad (14)$$

The r.h.s. of the above equation is entirely dependent on the present state of strain along the sample but not on the strain rate; therefore, the values of the strain rate $\dot{\varepsilon}_i$ can be calculated directly and integrated over the time step δt corresponding to a given increment of length δL. The adjustment of these steps was not imposed *a priori*. In this work, it was preferred to adjust it dynamically in the course of the computation in such a way that the true strain increment in the slice with the highest strain rate was held constant ($\delta\varepsilon_i=0.03$). By this means, the computing time is minimized for a given accuracy. It is clear that the maximum strain rate along the specimen depends substantially on the kinetics of flow localization. Under conditions in which the deformation is becoming sharply localized, the increment of total specimen

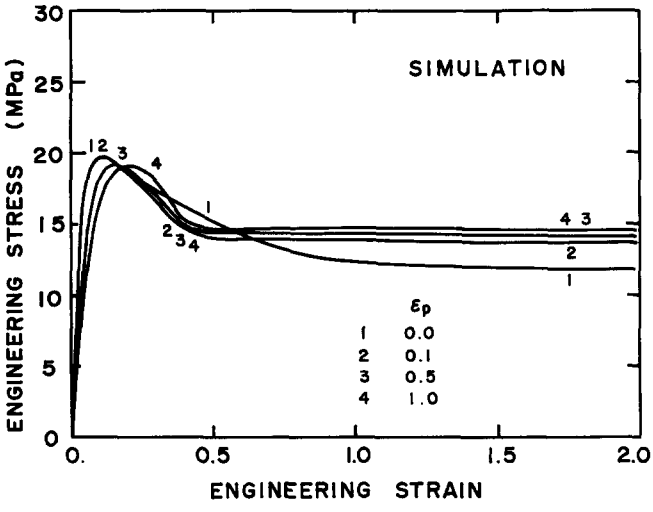

Figure 12 Simulated engineering stress–strain curves obtained from the computations for the same prestrains as in the experiments of *Figure 2*

elongation is reduced. Conversely, δL can be adjusted to a larger value (saving time) when the deformation rate is more uniform.

The number of elements was chosen equal to 100. In the case of samples with a localized predeformation, it was shown experimentally (*Figure 3*) that the observed secondary neck forms and develops first on one side of the central defect. This evolution was probably due to an undetected taper in the initial sample. For these cases, the diameter of the simulated sample was increased by 2.5% from the centre to one end of the specimen.

The program was written in the Microsoft Quick-Basic language and run on a PC-AT compatible microcomputer. The specimen profiles were drawn on a Hewlett-Packard digital plotter.

Results of the simulations

The engineering stress–strain curves obtained with the simulation code are displayed in *Figure 12* for the same set of prestrains, $\varepsilon_p = 0.0$, 0.1, 0.5 and 1.0, as for the experimental results of *Figure 2*. It is interesting to note that all the features of the experimental curves are reproduced by the simulation, including (i) the slight increase in the yield strain with ε_p, (ii) the uncommonly slow stress drop for the sample that was no predeformed and (iii) the raising of the plateau stress level with ε_p.

Also striking is the resemblance of the simulated profiles (*Figures 13a* to *13d*) to the experimental photographs (*Figures 3a* to *3d*). It is evident that the number of slices introduced in the simulation (100) is sufficient for an accurate description of the initiation and propagation of the necks. Also, the experimental asymmetry of neck propagation (the neck travels first towards one end of the sample, then towards the other) is correctly reproduced by the slight taper introduced *a priori* in the lower half of the sample to simulate the irregularities supposedly present in the testpieces. Unlike the analytical results obtained with the long-wavelength approximation (*Figure 10*), it is now evident in the simulations that the strain gradients are realistically small, as can be assessed by comparing the maximum slopes of the specimen profiles on the experimental photographs *versus* those predicted by the simulations. As indicated above, the improvement in the precision of the modelling can be attributed to the introduction of the Bridgman triaxiality factor. This is in line with previous experiments[14], which demonstrated the critical importance of triaxiality effects with regard to plastic instability in polymeric materials.

Also, the simulation takes very neatly into account the neck nucleating effect of a moderate predeformation. As illustrated for example in *Figure 13b* for $\varepsilon_p = 0.1$, the incipient neck forms readily at the mechanical defect, although there is no local reduction of cross-sectional area at that location. It should be noted here that the slight excess taper in the lower half of the simulated specimens is *not* responsible for this particular neck initiation mode; simulations run with perfectly uniform cross sections show exactly the same type of neck localization at the mechanical defects.

Finally, it is remarkable that this simple finite-difference model simulates the hardening effect of large prestrains so well, as in *Figure 13c* at $\varepsilon_p = 0.5$. Here the concurrent effects of large prestrain hardening in the centre of the defect plus the small prestrain destabilizing tendency at its edges are responsible for the resulting two-step necking phenomenon, with initial growth at the defect and further more rapid development at its border. The situation is similar in *Figure 13d* for $\varepsilon_p = 1.0$, except that necking occurs *ab initio* at the borders of the predeformed region and not at the centre of the defect.

CONCLUSIONS

Tensile samples of high-density polyethylene were prepared with a predeformed zone by applying successive machining, prestretching and remachining sequences. Tensile tests performed on these specimens show that the mechanical defects hardly affect the engineering stress–strain curves, but have a dramatic influence on the shapes of the stretched specimens. It was observed in particular that: (i) early necking occurs at the defect if the prestrain is small or moderate, owing to the reduction of the anelastic tangent modulus induced by the plastic deformation of the polyethylene crystallites; and (ii) neck stabilization finally occurs at the defect, owing to the increased strain hardening caused by the predeformation. These phenomena were accurately reproduced by means of a finite-difference simulation code based on the constitutive equation of the material and the description of stress triaxiality within the neck through the Bridgman formula. It is of interest to note that the present results are specific to polymeric materials, no equivalent phenomena being observed in metals. They are intrinsically associated with the structural mechanisms taking place in polyethylene during plastic deformation (lamellar glide, fragmentation and rotation), which in turn control the anelastic softening and ultimate plastic hardening of this polymer.

ACKNOWLEDGEMENTS

The final version of this paper was prepared during the sabbatical leave of one of the authors (C. G'Sell) at the National Institute of Standards and Technology (Gaithersburg, Maryland, USA). This was made possible by the attribution of a Guest Researcher position by this institute and a NATO Fellowship. The authors are

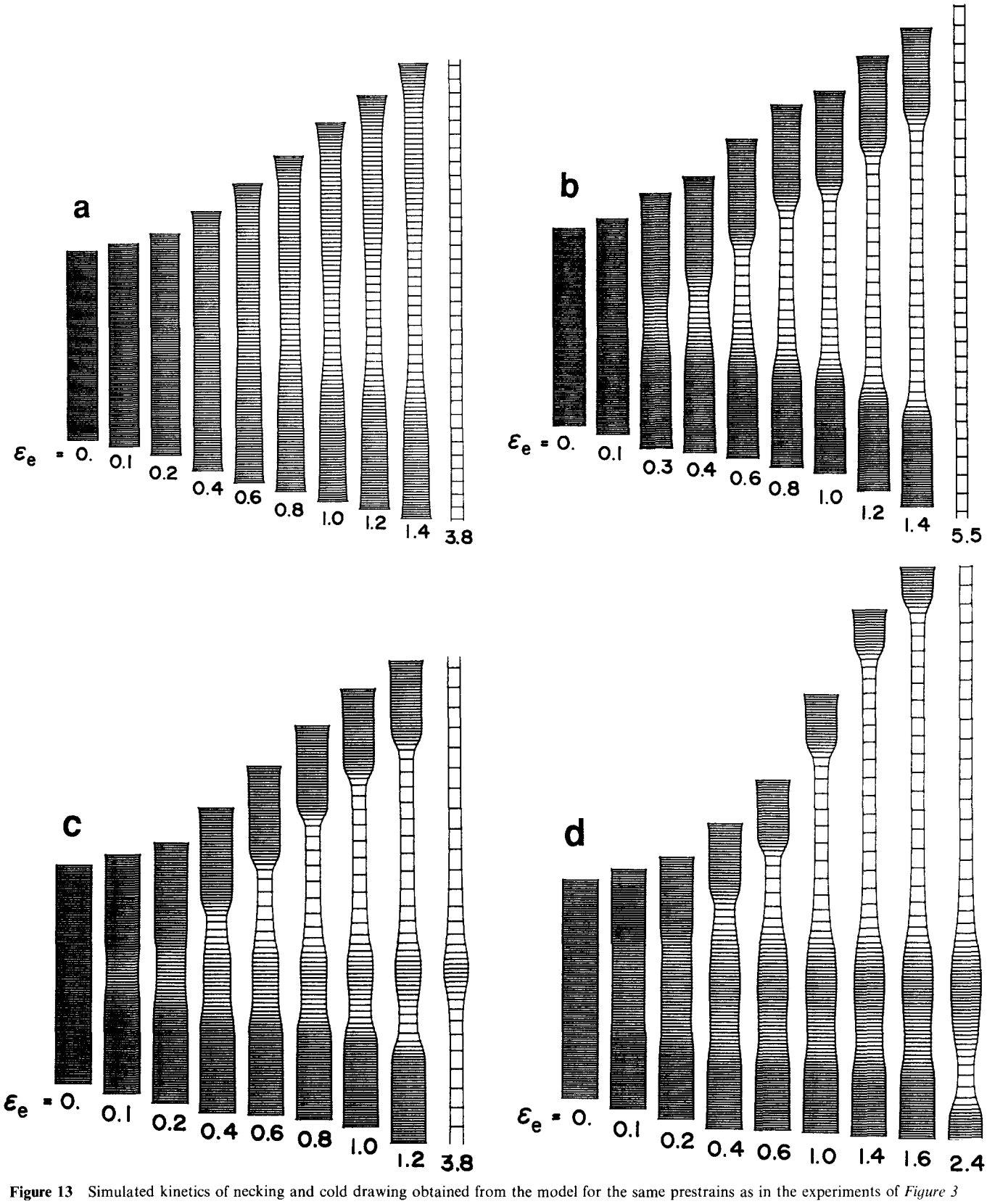

Figure 13 Simulated kinetics of necking and cold drawing obtained from the model for the same prestrains as in the experiments of *Figure 3*

grateful to Dr G. B. McKenna for valuable comments and suggestions on this work.

REFERENCES

1 Coffman, P. M. *Plast. Eng.* 1977, **8**, 18
2 Devries, A. J., Bonnebat, C. and Beautemps, J. *J. Polym. Sci., Polym. Phys. Edn.* 1977, **58**, 109
3 Brown, N., Duckett, R. A. and Ward, I. M. *Phil. Mag.* 1968, **18**, 483
4 Cotto, D., Montheillet, F. and Haudin, J. M. in 'Plastic Instability', Les Presses de l'Ecole Nationale des Ponts et Chaussées, Paris, 1985, p. 79
5 G'Sell, C. in 'Plastic Deformation of Amorphous and Semi-crystalline Materials' (Eds. B. Escaig and C. G'Sell), Les Editions de Physique, Les Ulis, 1982, p. 375
6 Rietsch, F., Duckett, R. A. and Ward, I. M. *Polymer* 1979, **20**, 1133

7 Peterlin, A. *J. Mater. Sci.* 1971, **6**, 490
8 Meinel, G., Morosoff, N. and Peterlin, A. *J. Polym. Sci., Polym. Phys. Edn.* 1970, **8**, 1723
9 Cross, A. and Haward, R. N. *J. Polym Sci., Polym. Phys. Edn.* 1973, **11**, 2423
10 Friedrich, K. in 'Crazing in Polymers' (Ed. H. H. Kausch), Springer-Verlag, Berlin, 1983, p. 225
11 Jones, J. J., Holt, R. A. and Coleman, C. E. *Acta Metall.* 1976, **24**, 911
12 Nichols, F. A. *Acta Metall.* 1980, **28**, 663
13 Semiatin, S. L. and Jones, J. J., 'Plastic Instability and Flow Localization', ASM, Metals Park, Ohio, 1984
14 G'Sell, C., Aly-Helal, N. A. and Jonas, J. J. *J. Mater. Sci.* 1983, **18**, 1731
15 G'Sell, C., Marquez-Lucero, A., Gilormini, P. and Jonas, J. J. *Acta Metall.* 1985, **33**, 759
16 G'Sell, C. and Jonas, J. J. *J. Mater. Sci.* 1979, **14**, 583
17 G'Sell, C. and Jonas, J. J. *J. Mater. Sci.* 1981, **16**, 1956
18 Bahadur, S. *Polym. Eng. Sci.* 1973, **13**, 266
19 Schultz, J. M., 'Polymer Materials Science', Prentice-Hall, Englewood Cliffs, NJ, 1974, p. 499
20 Weynant, E., Haudin, J. J. and G'Sell, C. *J. Mater. Sci.* 1982, **17**, 1017
21 Hart, E. W. *Acta Metall.* 1967, **15**, 351
22 Duncombe, E., *Int. J. Mech. Sci.* 1972, **14**, 325
23 Considère, A. *Ann. Ponts Chaussées* 1885, **9**, 574
24 Ford, H. *Proc. Inst. Mech. Eng.* 1948, **159**, 115
25 G'Sell, C., Marquez-Lucero, A., Souahi, A. and Tong, Y. S., in 'Plastic Instability', Les Presses de l'Ecole Nationale des Ponts et Chaussées, Paris, 1985, p. 159
26 Bridgman, P. W. *Trans. Am. Soc. Metals* 1944, **32**, 553
27 Mills, N. J. *Br. Polym. J.* 1978, **10**, 1
28 Semiatin, S. L., Ghosh, A. K. and Jonas, J. J. *Metall. Trans.* 1985, **16A**, 2291
29 Semiatin, S. L., Ayres, R. A. and Jonas, J. J. *Metall. Trans.* 1985, **16A**, 2299